A new methodology for muscle phenotyping by Raman spectroscopy

André Mourão Batista
Instituto de Pesquisas Energéticas e Nucleares
Diego Cunha Pascoal
Instituto de Pesquisas Energéticas e Nucleares
Paula Ketilly Nascimento Alves
Universidade de São Paulo
Luis Antonio Chinait Hess Costa Dutra
Universidade de São Paulo
Anselmo Sigari Moriscot
Universidade de São Paulo
Niklaus Ursus Wetter
Instituto de Pesquisas Energéticas e Nucleares
Anderson Zanardi Freitas
freitas.az.ipen@gmail.com

Instituto de Pesquisas Energéticas e Nucleares

Article

Keywords: skeletal muscle, fibers, Raman spectroscopy

Posted Date: June 6th, 2025

DOI: https://doi.org/10.21203/rs.3.rs-6657996/v1

Additional Declarations: No competing interests reported.

Abstract

Muscle fiber types perform distinct functions in skeletal muscle tissue, allowing a wide range of physical and motor capabilities. The characterization of these fibers is essential in several research fields, however, the methodologies currently used are quite expensive and time-consuming. Here we successfully demonstrate that Raman spectroscopy, combined with chemometric methods such as PCA, can distinguish different types of skeletal muscle fibers in the soleus muscle. Distinct spectral variations associated with tryptophan, phenylalanine, tyrosine, and the Amide I band were identified as critical biomarkers to differentiate fiber types. In addition, we highlight the structural changes of protein-related bands, demonstrating transitions and providing experimental evidence for conformational changes linked to muscle function. Our new methodology for detecting spectral patterns offers valuable insights into the biochemistry of muscle cells, enabling the identification of specific types of skeletal muscle fibers and paving the way for further investigations into these cells under various conditions, such as atrophy, hypertrophy, and sarcopenia.

Introduction

Skeletal muscle fibers are highly specialized cells responsible for voluntary movements and can be classified based on their contraction speed, metabolic properties, and fatigue resistance[1]. They can be divided into two main types, type I (TI) and type II (TII). Type I fibers are slow-twitch, highly oxidative, and fatigue-resistant, making them ideal for endurance activities. Type II fibers are fast-twitch and are further subdivided into Type IIa (oxidative glycolytic), Type IIx (glycolytic), and IIb (glycolytic and express the fastest twitch fiber). Type IIa fibers are moderately fatigue-resistant and are used in intermediate-duration activities, while Type IIx and IIb fibers are specialized for short bursts of high-intensity force but tire quickly. This diversity of muscle fiber types allows for a wide range of physical capabilities, from sustained endurance and body posture to rapid movements, which are essential elements for adequate environmental adaptation[2]. The characterization of these fibers is very important in several fields of research, such as in the understanding of cancer [3,4] in the early diagnosis of aging[5], in sports medicine[6], among others. Usually, those fibers are characterized by immunofluorescence-based assays utilizing specific primary and secondary antibodies, detecting the particular myosin heavy chain (MHC) expressed [7,8,9]. Although this method is considered quite precise, it requires a significant level of tissue preparation, it is time-consuming and the use of multiple antibodies makes it relatively expensive. In this sense, the characterization of novel methodologies able to identify those fibers is welcome.

Raman micro Spectroscopy (RμS) has emerged as a powerful and non-invasive analytical tool for the study of biological tissues, unraveling the molecular composition and structural information of various biomaterials [10,11]. This vibrational spectroscopy technique rests upon the inelastic scattering of monochromatic light, typically from a laser source, by molecular vibrations within a sample. The resulting Raman spectrum provides a wide range of information about the chemical environment, molecular interactions, and conformational states within the biological tissues being examined[12,13,14].

Moreover, RμS can characterize the presence of various biomolecules such as lipids, proteins, nucleic acids, and carbohydrates, allowing a better understanding of cellular functions and interactions within tissues[12,15,16]. This capacity to probe the biochemical landscape at single-cell resolution makes it an important tool in cell biology, enabling the characterization of heterogeneous populations of cells within tissues. This capability is particularly significant in the field of pathology, where differentiating between healthy and diseased tissues can be crucial for diagnosis and treatment planning[17,18,19]. For instance, the analysis of tissue sections can yield insights into the biochemical alterations associated with diseases such as breast cancer[17]. Raman spectral signatures can serve as biomarkers, identifying specific molecular changes that may indicate the presence or progression of malignancies.

Another significant advantage of RμS is its minimal sample preparation requirements. Traditional techniques, such as histology and immunohistochemistry, often rely on extensive labeling or fixation that may alter the intrinsic properties of the tissue. In contrast, the RμS allows for the analysis of fresh samples without time-consuming preparation, thus with an outstanding level of biomolecule preservation. Micro-Raman has been utilized to investigate skeletal muscle, mainly focusing on fiber optic-based assessment of the tissue in vivo to detect specific spectroscopic signatures in certain pathologies such as dystrophies, and muscle injury or addressing skeletal muscle-derived cell lines[20]. Those are valuable approaches to address skeletal muscle, nonetheless are limited in identifying specific skeletal muscle fiber Types. Here, we used the RμS associated with chemometrics to characterize specific muscle fiber types in tissue cross-sections with minimal preparation. The results showed that fiber-type phenotyping is possible.

Materials and Methods

Experimental Animals

Two wild male C57BL/6 mice, were kept in a temperature-controlled vivarium (more details in ethic statements), 24 ± 1°C, 12h light-dark cycle, standard food (Nuvilab CR-1, Nuvital-Quimtia, Brazil) and water offered *ad libitum*. This study was approved by the University of São Paulo (Institute of Biomedical Sciences) ethics committee under protocol # 2144240425 and followed the Code of Practice for the Housing and Care of Animals Used in Scientific Procedures.

Tissue preparation

The animals were deeply anesthetized and subjected to cervical dislocation. Subsequently, the soleus muscle was removed, and transversely sectioned into two equivalent fragments which were cryoprotected by cold isopentane for 1 minute, and immediately immersed in liquid nitrogen[21]. The tissue fragments were then cut (mirrored) in a cryostat at thicknesses of 10 μm, for prior characterization by immunofluorescence assays, and 50 μm for analysis by RμS (Fig. 1). They were subsequently applied on slides and fixed in a solution containing 4% paraformaldehyde for 10 min,

washed (3 times for 5 min) with TBS-T (tris-buffered saline, 0.5 M NaCl, 50 mM tris-HCl pH 7.4 with 0.3% TRITON X-100) and then mounted with a glycerol-based preparation.

Immunofluorescence assay

Slides were initially incubated with a blocking solution (MKB-2213, Vector Lab) for 1 hour, in PBS and then incubated overnight at 4 ºC with the following primary antibodies all from (Developmental Studies Hybridoma Bank, University of Iowa): anti-MHC I (#BA-D5, mouse IgG2b, 1:500), Anti-MHC IIa (#SC-71, mouse IgG1, 1:400); and diaphragm muscle membrane was stained using anti-dystrophin antibody (SC#15376, rabbit IgG, 1:500). The secondary antibodies: DyLight 405 goat anti-mouse IgG2b (Jackson ImmunoResearch, West Grove, PA, USA, #115-475-207, 1:200), Cy2 goat anti-mouse IgG1 (Jackson ImmunoResearch #115-225-205, 1:200), and Cy3 donkey anti-rabbit (Jackson ImmunoResearch #711-165-152, 1:200) were subsequently used for 1 h at 37°C. Photomicrographs (Fig. 1) were acquired using Axio Scope A1 (Carl Zeiss Microscopy GmbH, Göttingen, Germany).

Raman Spectrometer

A confocal Raman spectrometer, LabRam HR Evolution HORIBA Scientific, was used with a 50x magnification objective and a 473 nm excitation laser wavelength, with a power of 12.74 mW on the sample, pinhole of 100 µm, integration time of 5 s, and using a diffraction grating of 600 l/mm. The positioning of the focus of the objective at 5 microns below the sample's surface to avoid coverslip fluorescence. For each cell 40 spectra were collected in the region of 500 to 3600 cm^{-1}, 20 in the central area of the muscle cell, and 20 in the peripheral area (Fig. 1).

Experimental setup

The experiment consisted of the *ex vivo* analysis of the soleus muscle, which was dissected and removed so that its mass could be measured. The muscle mass parameter was normalized using the muscle mass/body mass ratio of the animal. Then the immunofluorescence assay was performed first to characterize the fiber types, and subsequently, the spectroscopic and statistical/chemometric analyses were taken.

Data processing

After collecting 40 spectra per cell, the raw data were processed using LabSpec 6 software, performing spike removal, noise reduction by applying 8-neighbor polynomial smoothing, baseline application using a 4-point polynomial method, and normalization by the spectral range of 2800 to 3100 cm^{-1} (peak of highest intensity). Origin Pro 8.5, Fityk, and RStudio software were also used to plot, analyze, and fit the experimental data.

Statistical Analysis

Dimensionality reduction of the spectral data was performed by principal component analysis (PCA) through the R language, using the RStudio program. The ChemoSpec package was used for multivariate analyses. The distributions of intensity ratios were plotted in boxplots and multiple pairwise comparisons between fiber types were performed using the Kruskal-Wallis test and non-paired Wilcox's test, and correlation studies were analyzed.

Results and Discussion

The main objective of our study was to analyze the three specific types I, IIa, and IIx of skeletal muscle fibers present within the soleus muscle to identify distinct RμS spectral signatures. These fibers were previously characterized by a standard immunofluorescence assay. This work enhances the understanding of the chemical constituents of these cells and potentially facilitates the identification of specific fiber types, independently of classical detection methods such as Myosin Heavy Chain immunolabeling. The following sections will specifically address the analyses performed cells.

PCA in the spectral range 500–3600cm^{-1}

Initially, a spectral pattern was sought to distinctly characterize each type of fiber to perform phenotyping using the Raman spectroscopy technique. The key constituents and vibrational modes associated with these fibers are summarized in Table 1 (and Extended Data Table 1). To this end, 40 measurements were taken from over 150 cells, totaling 6000 spectra. However, contamination from mandatory chemical agents used in the coverslip fixation process—specifically glycerol—interfered with the spectra, reducing the number of usable samples to 105 cells. At first glance, it was challenging to distinguish between the fiber types without further assistance, however, a more evident distinction emerged between type I and type II fibers utilizing specific chemometric tools, as described below.

A statistical analysis was performed using PCA on the generated spectra clusters to differentiate these fibers further. As shown in Fig. 2, the spectra are largely similar, resulting in peak overlap (Fig. 2a). The loading plots of the first two principal components (Figs. 2b - c) revealed certain anomalous interferences in the high-frequency region (3000–3600 cm^{-1}) but highlighted the greatest spectral variation in the region between 1500 and 1800 cm^{-1}. The 3D PCA plots (Fig. 2d) indicate some clustering tendency, despite considerable dispersion. Notably, two large clusters were observed, which we attribute to the anomalous spectral features in the high-frequency region above 3000 cm^{-1}.

For the above reasons, we decided to restrict the spectral range under investigation and focus on the region between 1500 and 1800 cm^{-1}, using the cell average to minimize the observed spectral dispersion.

PCA in the spectral range 1500–1800 cm^{-1}

Within this narrower range, spectral differentiation between type I and type II fibers became apparent (Figs. 3a–b). Notably, a nearly equal intensity is observed between the 1600 and 1657 cm^{-1} bands for type I fibers, while a marked increase in intensity is seen in the 1600 cm^{-1} band for type II fibers. This intensity variation was most pronounced in type IIa fibers. The loading plots of principal components (PCs) 1 and 2 (Fig. 3c) further highlight the regions of greatest spectral variation, specifically between 1590 and 1604 cm^{-1} for PC1 and 1650 to 1670 cm^{-1} for PC2; these spectral features correspond to vibrations associated with tryptophan, phenylalanine, tyrosine, and amide I (Table 1). These chemical agents, mainly amino acids, are intrinsically linked to cellular biochemical processes, where they play crucial roles in muscle cell metabolism[22,23,24]. Specifically, they are notably involved in protein synthesis, therefore, in growth, in force generation, all of which influence the performance, endurance, and structural integrity of muscle fibers[25].

The spectral region between 1590 and 1604 cm^{-1} may also be associated with nucleic acids [26], e.g., RNA, which plays a crucial role in muscle function. As is well established [27,28], ribosomal and messenger RNAs are directly involved in protein synthesis. Therefore, the increased intensity of this band in type II muscle fibers can be interpreted as a result of elevated levels of amino acids and ribosomal/messenger RNA in these fibers. However, existing literature also suggests that this nucleic acid content is actually higher in type I fibers[29], indicating that the band in question may not specifically reflect ribosomal or messenger RNA content. It is plausible that DNA, rather than RNA, contributes to the observed intensity of this particular band. It is important to note that the variability in spectral intensity within the same fiber is significant. This variation may be attributed to activity cycles, potentially reflecting fluctuations in protein synthesis levels, such as periods of lower and higher synthesis[30, 31] The main finding was observed in the three-dimensional graphs (Fig. 3d), where a distinct separation/grouping was observed between the confidence ellipses between the three types of fibers, showing that it is possible to perform muscle phenotyping.

Intensity ratio analysis is a widely employed technique in vibrational spectroscopy [32,33,34], including in biological assays[35]. In the present study, the ratios between the intensities of the frequencies/wavenumber of the amino acids: tryptophan, phenylalanine, and amide I (1359, 1601–1604, and 1657 cm^{-1}, respectively) were analyzed to differentiate the fiber types. These specific frequencies showed considerable variations in intensity, as depicted in Fig. 4a.

This spectral analysis facilitated the separation of the three fiber types for both animals (Fig. 4b), even considering the propagation of errors in the calculations. Notably, the error bars do not overlap for the same animal sample. Another observation is that in one of the animals the intensity ratio values, in both ratios evaluated, exhibited a greater distance, that is, the separation/distance by fiber type is even greater, causing a more pronounced slope between the data points. This phenomenon may arise from biological variations between animals in the abundance of agents that compose the 1604 cm^{-1} band, or from the intracellular biochemical variability already discussed. Since the main components of the 1604 cm^{-1} band are amino acids, notably crucial for skeletal muscle fiber homeostasis, one can imagine that

these variations may reflect stages of fiber turnover, where free amino acids float within the cell. However, in the correlation analysis (Fig. 4c), the intensity of the 1604 and 1657 cm-1 bands showed a high degree of correlation.

Muscle cells were also studied by the mean distribution of the 1601/1359 and 1604/1657 cm-1 ratio, where Fig. 4d - e shows that the profile of the cells is similar. TI fibers have a lower ratio intensity, while TIIa and TIIx fibers have a higher ratio intensity, with a statistically significant difference between the cell fiber types.

Another factor/parameter used to observe small spectral variations is the bandwidth, which can be evaluated through theoretical fits of the experimental data. In this context, four Gaussian functions were applied in the range of 1500 to 1750 cm-1 to represent the experimental data for quantitative analysis (Fig. 5). In these quantitative analyses, the area value of four Gaussians representing the tryptophan, phenylalanine/tyrosine and Amide I bands, respectively, was first observed (Fig. 5a), where their area values are described within the bands in question. A significant increase in the area of the phenylalanine/tyrosine band (TI < TIIA < TIIx) can be observed. In the spectral region of amide I, two bands of the secondary structure of myosin were evaluated, one at 1657 cm-1 representing the α-helix structure and the other at 1685 cm-1, representing the β-sheet structure[36, 37], in these regions there was an increase in the alpha structures and a decrease in the β-sheet structure in the direction of type I to type IIx fibers. Figure 4b shows the Half-Width at Half-Maximum (HWHM) behavior of the fits for the band near 1604 cm-1, where a distinct separation between fibers is evident, as the error bars do not overlap, revealing the unique characteristics of each fiber.

This spectral region corresponds to three specific amino acids, tyrosine, tryptophan, and phenylalanine (Table 1), indicating that these are the main chemical components responsible for fiber differentiation. As already mentioned above, fluctuations in the levels of these intrafiber-free amino acids can impact trophicity in relation to cycles of more or less intense protein synthesis activity. Indeed, phenylalanine, which is the most predominant and most variable chemical component of the 1604 cm^{-1} band, can induce protein synthesis by activating the PI3K/AKT/mTOR pathway, a key mechanism involved in maintaining skeletal muscle fiber size and strength [38].

These findings provide great experimental insights into muscle fibers, especially because they help to understand conformational changes related to protein secondary structures. To our knowledge, such data have not yet been reported in the literature.

Table 1
The spectral interpretations

Frequency (cm^{-1})	Compounds	Vibrational Bonds / Assignement
1359	Tryptophan (1360) [35,39]	ν ring
1552	Tryptophan (1552–1555) [40]	ν (C = C), tryptophan (protein assignment)
1577	Nucleic Acids, A, G (1576) [39,41]	
1592	Phenylalanine (1580–1599) [39,42] / Nucleic acids (1592) [26]	C = N and C = C stretch. in quinoid ring
1601	Phenylalanine (1601–1604) [39,40,43]	Phenylalanine (protein assignment), Ring C-C stretch. of phenyl, δ (C = C)
1605	Phenylalanine (1605–1607) [39] / Tyrosine (1607) [44]	Ring C-C stretch of Phenyl / Tyr ν ring / C = C in-plane bending mode of phenylalanine & tyrosine
1615–1618	Tyrosine (1614–1617) [39,43] / Tryptophan (1615–1623) [39,40]	C = C stretching mode / ν Cα - Cβ.
1620–1750	Amide I [20,36, 37,39]	Stretch. C = C of Amide I (1650) / Lipid (1652–1655) / Carbonyl stretch. C = O (1653) / T, G, C ring breathing modes of the DNA/RNA (1655–1680) / α-helix structure C = O stretching mode (1657) / β-sheet structure (1685)
ν - stretching vibration		
δ – deformation vibration		

Conclusions

This study successfully demonstrated that Raman spectroscopy, combined with chemometric methods such as PCA, can distinguish different types of skeletal muscle fibers in the soleus muscle. Despite challenges like spectral contamination from the fixation process agents and overlapping vibrational peaks, clear patterns emerged within specific spectral bands, particularly near the Amide I region (1500–1800 cm^{-1}). Distinct spectral variations associated with tryptophan, phenylalanine, and tyrosine were identified as critical markers for differentiating fiber types. These amino acids directly influence metabolism, protein synthesis, and maintenance of muscle cells.

Despite the variations in spectral patterns, it can be seen that the fiber type pattern was repeated for both animals, where the TI fiber showed weaker intensity in the amino acid bands than the TIIa and TIIx

fibers. We also highlight changes in protein secondary structure, demonstrating a structural transition and providing experimental evidence for conformational changes linked to muscle function. Intensity ratios and bandwidth analysis were also shown to further validate the distinction of fiber types, with no overlapping error bars, indicating reliable statistical differentiation. Studies related to the accuracy of this methodology are currently being carried out.

Our findings establish Raman spectroscopy as a powerful methodology to identify and characterize specific skeletal muscle fibers. This novel methodology for detecting spectral patterns offers valuable insights into muscle cell biochemistry, enabling the identification of specific skeletal muscle fiber types and paving the way for new investigations into these cells under various conditions, such as atrophy, hypertrophy, and sarcopenia.

Declarations

Competing Interests

The authors declare no competing interests.

Ethic statements

All animal handling procedures were carried out by trained personnel at the animal facilities of our institute, following approval by the Ethics Committee on the Use of Animals (CEUA) of the Institute of Biomedical Sciences, University of São Paulo (Protocol No. 2144240425). All experimental procedures were conducted in accordance with Brazilian national legislation (Law No. 11,794/2008), the guidelines of CONCEA (National Council for the Control of Animal Experimentation), and the DBCA (Brazilian Guidelines for the Care and Use of Animals for Scientific and Educational Purposes). This study also adhered to relevant international standards, and all methods are reported in accordance with the ARRIVE guidelines (https://arriveguidelines.org).

Author Contribution

A.Z.F., N.U.W., and A.S.M. conceived the project, supervised the research, and wrote the manuscript. P.K.A. and L.C.D. established the conditions, prepared the slides accessed by RAMAN, and performed immunofluorescence assays. A.M.B., D.C.P., and A.Z.F. performed the characterizations and analyses related to Raman microspectroscopy. D.C.P. and A.M.B. developed and improved the multivariate analysis code in R language for statistical analyses, and wrote the manuscript. All authors contributed to the discussion and review of the article.

Acknowledgments

The authors would like to thank the Institute of Energy and Nuclear Research (IPEN) and the Institute of Biomedical Sciences of the State University of São Paulo (ICB/USP) for all their technical/scientific support. We thank Kelly P Borges for excellent technical advice. We would also like to thank the FAPESP grant n. 2018/19240-5, 2023/04564-8, 2024/07162-0, and CNPq grant n. 314079/2021-1.

Data Availability

If this manuscript is considered for publication, all data and code will be made available in an online repository (https://datarepository.ipen.br/)

References

1. Scott, W., Jennifer, S. & Stuart, A. B. Human skeletal muscle fiber type classifications. *Phys. Ther.* **81**, 1810–1816 (2001).
2. Zhang, W., Yuan, L. & Hong, Z. Extracellular matrix: an important regulator of cell functions and skeletal muscle development. *Cell biosci* **11**, (2021).
3. Martin, A. & Damien, F. Phenotypic features of cancer cachexia-related loss of skeletal muscle mass and function: lessons from human and animal studies. *JCSM* **12**, 252–273 (2021).
4. Anoveros-Barrera, A. et al. Clinical and biological characterization of skeletal muscle tissue biopsies of surgical cancer patients. *JCSM* **10**, 1356–1377 (2019).
5. Dowling, P. et al. Fiber-type shifting in sarcopenia of old age: proteomic profiling of the contractile apparatus of skeletal muscles. *Int. J. Mol. Sci.* **24**, 2415 (2023).
6. Deschenes, M. R. Effects of aging on muscle fiber type and size. *Sports Med.* **34**, 809–824 (2004).
7. Englund, D. A. et al. p21 induces a senescence program and skeletal muscle dysfunction. *Mol. Metab.* **67**, 101652 (2023).
8. Rodrigues, M. R. & de Camargo *Efeitos da inibição farmacológica de MuRF1 em associação a eletroestimulação neuromuscular na massa e força do músculo esquelético* (Diss. Universidade de São Paulo, 2023). https://www.teses.usp.br/teses/disponiveis/42/42134/tde-05022024-134049/en.php
9. Fuerniss, L. K. & Bradley, J. J. Semi-automated technique for bovine skeletal muscle fiber cross-sectional area and myosin heavy chain determination. *J Anim. Sci* 101 (2023).
10. Zhang, Y. et al. Optical penetration of surface-enhanced micro-scale spatial offset Raman spectroscopy in turbid gel and biological tissue. *J Innov. Opt. Health Sci* **14**, (2021).
11. Batista, A. M. et al. Advances in tissues and cells characterization by Raman micro-spectroscopy, atomic force microscopy, and tip-enhanced Raman spectroscopy. *J. Raman Spectrosc.* **53**, 1848–1860 (2022).
12. Kuhar, N., Sanchita, S. & Siva, U. Potential of Raman spectroscopic techniques to study proteins. *Spectrochim Acta Part. Mol. Biomol. Spectrosc* **258**, (2021).

13. Bonhommeau, S., Gary, S. C. & Yuhan, H. Nanoscale chemical characterization of biomolecules using tip-enhanced Raman spectroscopy. *Chem. Soc. Rev.* **51**, 2416–2430 (2022).
14. Plou, J. et al. Prospects of surface-enhanced Raman spectroscopy for biomarker monitoring toward precision medicine. *ACS photonics*. **9**, 333–350 (2022).
15. Bonhommeau, S., Gary, S. C. & Yuhan, H. Nanoscale chemical characterization of biomolecules using tip-enhanced Raman spectroscopy. *Chem. Soc. Rev.* **51**, 2416–2430 (2022).
16. Plou, J. et al. Prospects of surface-enhanced Raman spectroscopy for biomarker monitoring toward precision medicine. *ACS photonics*. **9**, 333–350 (2022).
17. Ning, T. et al. Raman spectroscopy based pathological analysis and discrimination of formalin fixed paraffin embedded breast cancer tissue. *Vib Spectrosc* **115**, (2021).
18. Cutshaw, G. et al. The emerging role of Raman spectroscopy as an omics approach for metabolic profiling and biomarker detection toward precision medicine. *Chem. Rev.* **123**, 8297–8346 (2023).
19. Qi, Y. et al. Applications of Raman spectroscopy in clinical medicine. *Food Front.* **5**, 392–419 (2024).
20. Plesia, M. et al. In vivo fiber optic Raman spectroscopy of muscle in preclinical models of amyotrophic lateral sclerosis and Duchenne muscular dystrophy. *ACS Chem. Neurosci.* **12**, 1768–1776 (2021).
21. Silva, W. J. et al. miR-29c improves skeletal muscle mass and function throughout myocyte proliferation and differentiation and by repressing atrophy-related genes. *Acta Physiologica* 226 (2019).
22. Jeong, H. et al. Effect of Phenylalanine on Differentiation of Myoblast C1C12 and L6 Cells Into Myocytes. *Food Suppl. Biomater. Health* **3**, (2023).
23. Hollenberg, M. D. Tyrosine kinase pathways and the regulation of smooth muscle contractility. *Trends Pharmacol. Sci.* **15**, 108–114 (1994).
24. Moffett, J. R. Tryptophan and the immune response. *Immunol. Cell. Biol.* **81**, 247–265 (2003).
25. Tipton, K. D. Exercise, protein metabolism, and muscle growth. *Int. J. Sport Nutr. Exerc. Metab.* **11**, 109–132 (2001).
26. Ong, Y. H., Mayasari, L. & Quan, L. Comparison of principal component analysis and biochemical component analysis in Raman spectroscopy for the discrimination of apoptosis and necrosis in K562 leukemia cells. *Opt. Express*. **20**, 22158–22171 (2012).
27. Yusupova, G. Z. et al. The path of messenger RNA through the ribosome. *Cell* **106**, 233–241 (2001).
28. Brenner, S., François, J. & Matthew, M. An unstable intermediate carrying information from genes to ribosomes for protein synthesis. *Nature* **190**, 576–581 (1961).
29. Habets, P. et al. RNA content differs in slow and fast muscle fibers: implications for interpretation of changes in muscle gene expression. *J. Histochem. Cytochem.* **47**, 995–1004 (1999).
30. Snijder, B. & Lucas, P. Origins of regulated cell-to-cell variability. *Nat. Rev. Mol. Cell. Biol.* **12**, 119–125 (2011).

31. Schwabe, A. et al. Origins of stochastic intracellular processes and consequences for cell-to-cell variability and cellular survival strategies. *Methods Enzymol.* **500**, 597–625 (2011).
32. Munoz, T., Jose, A. & Marc, J. A. Quantitative analysis of monoclinic phase in 3Y-TZP by Raman spectroscopy. *J. Am. Ceram. Soc.* **93**, 1790–1795 (2010).
33. Shin, W. S. et al. Determination of the degree of cure of dental resins using Raman and FT-Raman spectroscopy. *Dent. Mater.* **9**, 317–324 (1993).
34. Jiang, J. et al. A Raman spectroscopy signature for characterizing defective single-layer graphene: Defect-induced I (D)/I (D') intensity ratio by theoretical analysis. *Carbon* **90**, 53–62 (2015).
35. Herrero, A. M. Raman spectroscopy for monitoring protein structure in muscle food systems. *Crit. Rev. Food Sci. Nutr.* **48**, 512–523 (2008).
36. Carew, E. B. et al. Studies of myosin and its proteolytic fragments by laser Raman spectroscopy. *Biophys. J.* **44**, 219–224 (1983).
37. Adar, F. Interpretation of Raman spectrum of proteins. 9 (2022).
38. Yoshida, T. & Patrice, D. Mechanisms of IGF-1-mediated regulation of skeletal muscle hypertrophy and atrophy. *Cells* **9**, 1970 (2020).
39. Talari, A. C. S. et al. Raman spectroscopy of biological tissues. *Appl. Spectrosc. Rev.* **50**, 46–111 (2015).
40. Huang, Z. et al. Near-infrared Raman spectroscopy for optical diagnosis of lung cancer. *Int. J. Cancer*. **107**, 1047–1052 (2003).
41. ThomasJr & George, J. Raman spectroscopy of protein and nucleic acid assemblies. *Annu. Rev. Biophys. Biomol. Struct.* **28**, 1–27 (1999).
42. Freire, P. T. et al. Raman spectroscopy of amino acid crystals. *Raman Spectrosc. Applications* **201** (2017).
43. Cheng, W. et al. Micro-Raman spectroscopy used to identify and grade human skin pilomatrixoma. *Microsc Res. Tech.* **68**, 75–79 (2005).
44. Lakshmi, R. J. et al. Tissue Raman spectroscopy for the study of radiation damage: brain irradiation of mice. *Radiat. Res.* **157**, 175–182 (2002).
45. Gautam, R. et al. Review of multidimensional data processing approaches for Raman and infrared spectroscopy. *EPJ Tech. Instrum.* **2**, 1–38 (2015).

Figures

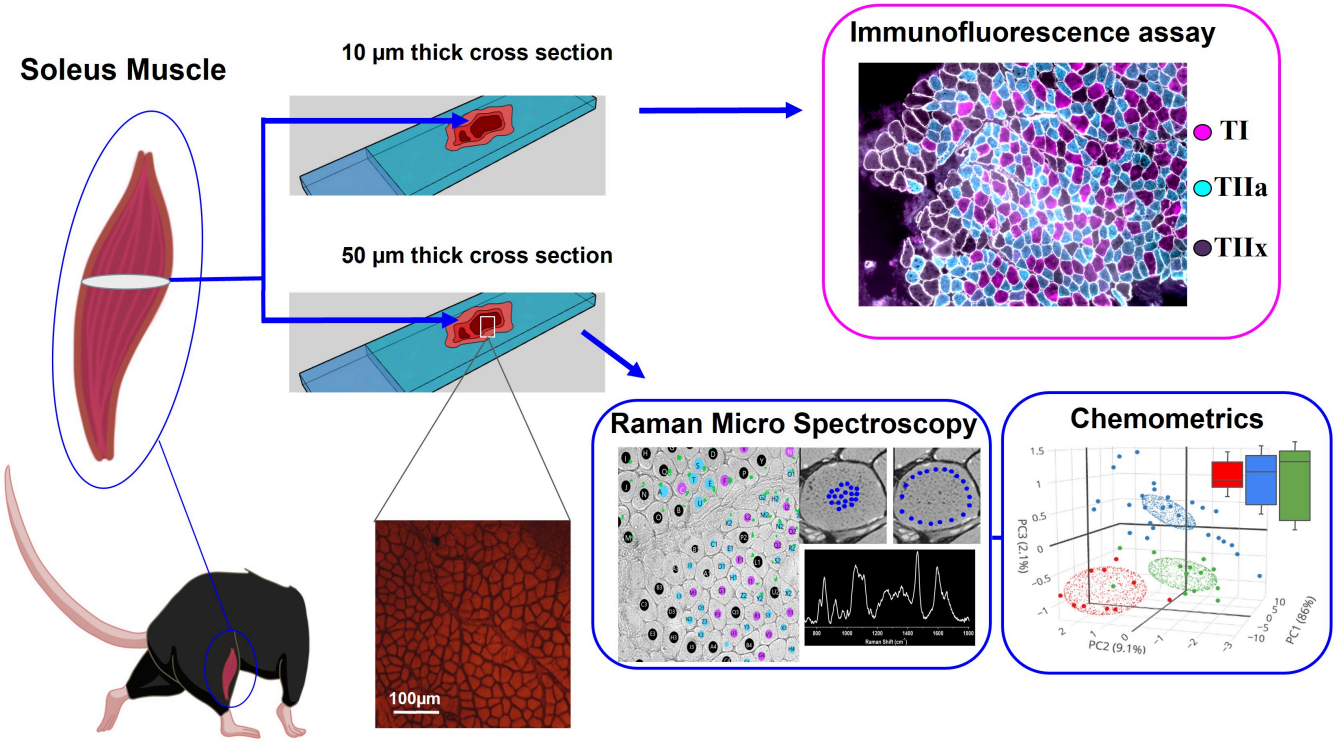

Figure 1

Schematic representation of the experimental and statistical procedures.

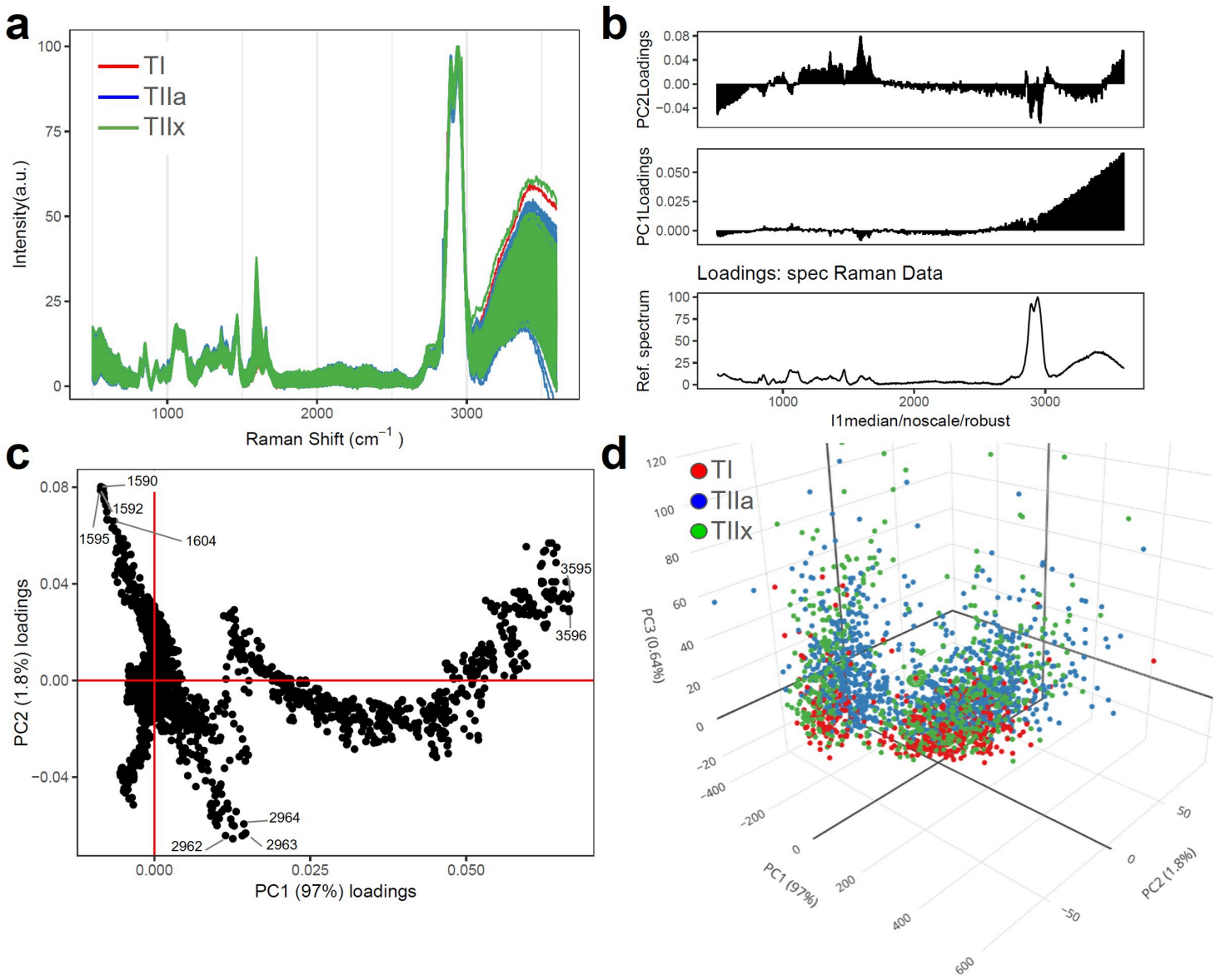

Figure 2

PCA data in the spectral range 500 - 3600 cm^{-1} for the 40 points per cell, where: **a)** Raman spectra of fibers TI, TIIa, TIIx; **b)** and **c)** Loading of the spectral variation observed of the principal components 1 and 2; **d)** 3D PCA plot of fibers.

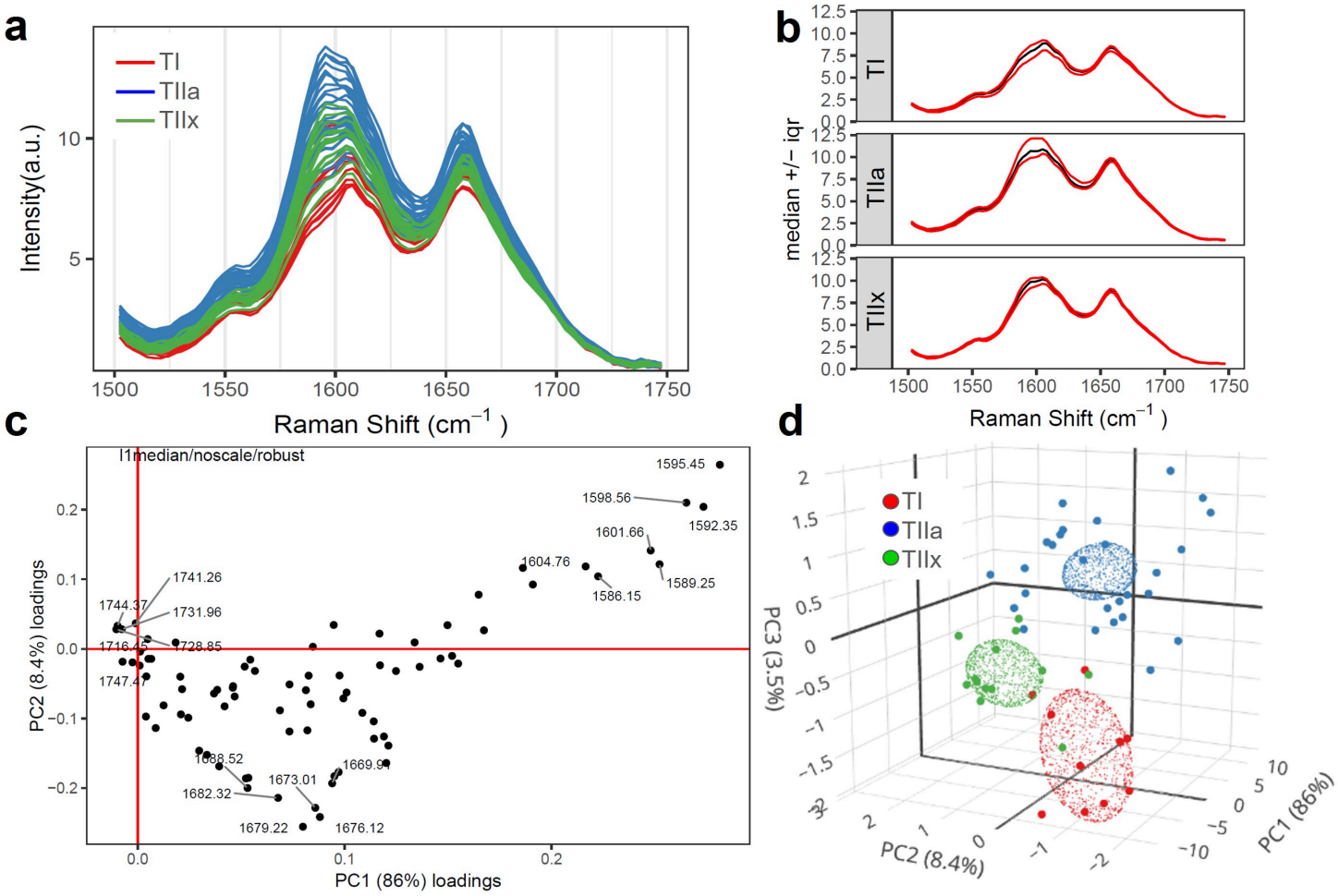

Figure 3

PCA data in the spectral range 1500 - 1800cm^{-1} for the cell averages, where: **a)** Raman spectra of TI, TIIa, TIIx fibers; **b)** Median variation for each fiber type separately; **c)** Loading of the observed spectral variation of principal components 1 and 2; **d)** 3D PCA plot of fibers.

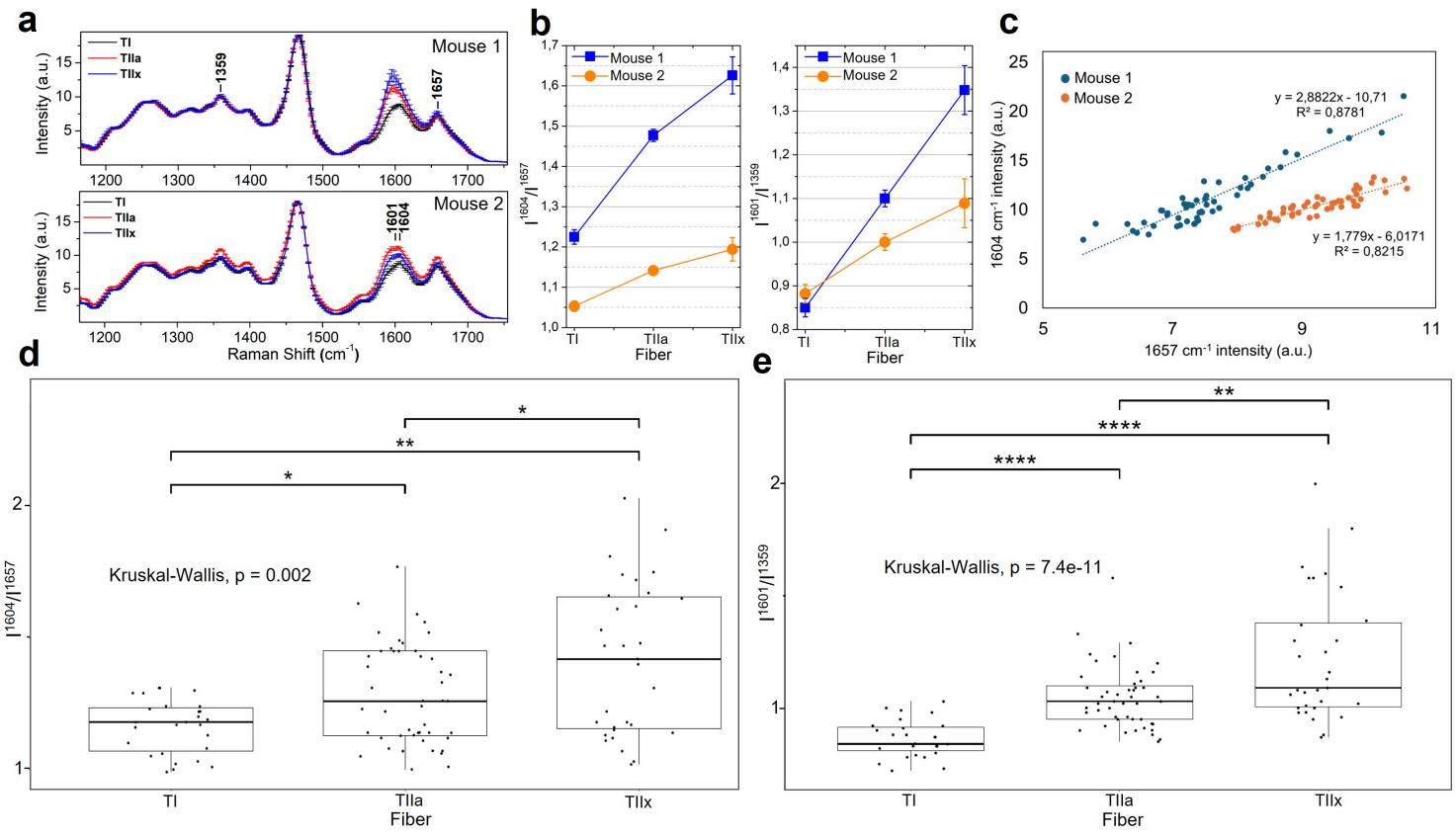

Figure 4

a) Average Raman spectra by fiber Type of all analyzed cells with the standard error. **b)** Analysis of the ratio between the intensities of the 1604/1657 and 1601/1359 cm^{-1} bands for the two mice separately. c) Correlation between average intensities of 1604 and 1657 cm^{-1} of each cell. d) Boxplot of the average ratios of 1604/1657. e) Boxplot of the average ratios of 1601/1359 per cell. Where in the Wilcox's test: * $p \leq 0.05$, ** $p \leq 0.01$, **** $p \leq 0.0001$).

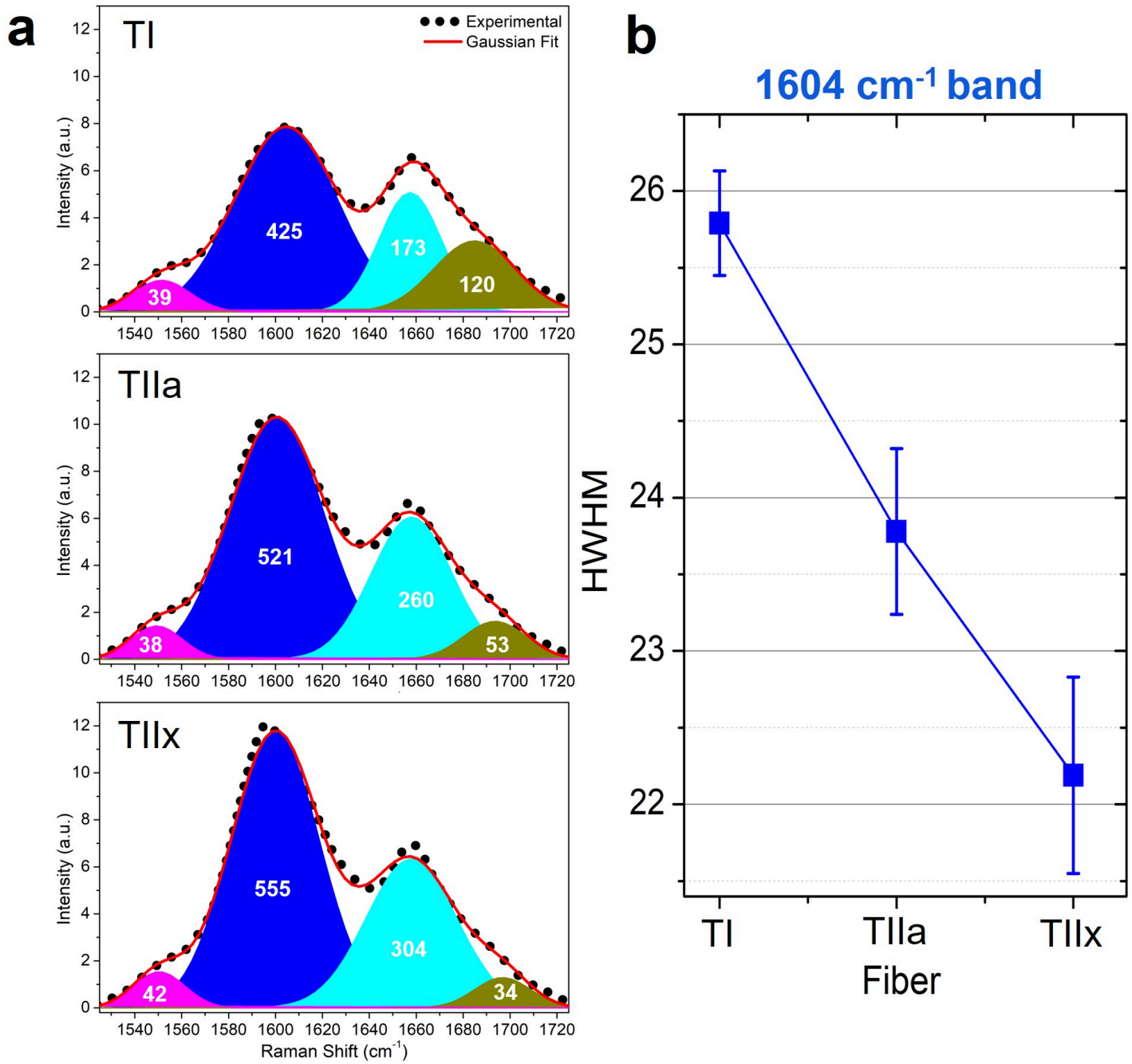

Figure 5

a) Gaussian fittings of the bands in the region 1500 - 1800cm^{-1}. The numbers inside the bands refer to the area values. **b)** HWHM analysis of the 1604 cm-1 band of figure a

Supplementary Files

This is a list of supplementary files associated with this preprint. Click to download.

- Extendeddata.docx